Exact normal forces and trajectories for a rotating tripod sliding on a smooth surface

Mark R.A. Shegelski, Glen L. Goodvin, Rebecca Booth, Peter Bagnall, and Matthew Reid

Abstract: We study the motion of a rotating tripod sliding over a smooth surface. The tripod is important and unique in that it is the only case where all aspects of the motion can be solved exactly. From the three constraint equations, we calculate the three normal forces and friction forces, which we then use to calculate the trajectory and other physical quantities of interest. We report novel results: the normal force has an interesting form when the sliding speed and the speed of rotation are almost equal; the tripod can execute serpentine trajectories; trajectories can have large lateral deflections; the translational kinetic energy can decrease and increase during a full rotation; the tripod can tip at a very late stage of its motion. The tripod trajectories are compared to trajectories of rotating, sliding cylinders that have continuous contact rings. We discuss significant implications of our results.

PACS No.: 45.40.–f

Résumé : Nous étudions le mouvement d'un tripode en rotation et glissant sur une surface lisse. Le cas du tripode est important, parce que c'est le seul cas où tous les aspects du mouvement peuvent être résolus exactement. À partir des trois équations de contrainte, nous calculons les trois forces normales et les forces de friction, qui sont ensuite utilisées pour déterminer la trajectoire et évaluer les quantités d'intérêt physique. Nous présentons de nouveaux résultats : la force normale prend une forme intéressante lorsque la vitesse de rotation et celle de glissement sont presque égales ; le tripode peut exécuter des trajectoires serpentines ; les trajectoires peuvent présenter des déplacements latéraux importants ; l'énergie cinétique de translation peut diminuer et augmenter sur un cycle de rotation ; le tripode peut se renverser vers la toute fin de son mouvement. Nous comparons les trajectoires des tripodes avec celles de cylindres glissant en tournant et dont les lieux de contact sont des cercles continus. Nous analysons les implications de nos résultats.

[Traduit par la Rédaction]

Received 19 July 2004. Accepted 13 October 2004. Published on the NRC Research Press Web site at http://cjp.nrc.ca/ on 17 November 2004.

M.R.A. Shegelski,[1] G.L. Goodvin, R. Booth, and P. Bagnall. Department of Physics, University of Northern British Columbia, 3333 University Way, Prince George, BC V2N 4Z9, Canada.
M. Reid. Department of Electrical and Computer Engineering, University of Alberta, 2nd Floor ECERF, Edmonton, AB T6G 2V4, Canada.

[1]Corresponding author (e-mail: mras@unbc.ca).

 doi: 10.1139/P04-062

1. Introduction

In this paper, we investigate the motion of a sliding, rotating tripod. This is a unique case in that it is the only sliding, rotating object for which all aspects of the motion can be calculated exactly, with no approximations. To accurately predict the motion of a sliding object, the contact geometry and pressure distribution are critical parameters that require either an experimental evaluation or a solid theoretical prediction [1,2]. Indeed, the real contact area of a sliding object is one of the main concerns in the friction of unlubricated solids [3]. In the present study, the trajectory and associated normal force distribution for a tripod are examined analytically, without the need to assume any pressure distribution. Further, it is shown that the motion of a continuous contact ring can be approximated, under certain physical conditions, by that of a tripod. This has implications regarding the calculation of trajectories for more complicated sliding contact rings, such as curling rocks [4–16].

We calculate the exact normal forces on the three legs of the tripod and derive the equations of motion for the tripod with only basic assumptions. The possible trajectories we report have novel features. For example, in the rapid rotation regime, we find "looping" trajectories where the tripod is found to curve through large angles. The extreme case yields nearly circular loops. We show that the tripod can follow serpentine paths; for example, the tripod can curl to the right and then back to the left during its motion. Such serpentine paths show oscillations in the lateral direction of motion and can even end with a sudden reversal in lateral direction. We find that the *translational* kinetic energy of the tripod can oscillate: increasing and decreasing over a full rotation, while still being monotonically decreasing over any full cycle of rotation. When the translational speed of the center of mass (CM) and the speed of rotation of the contact points are almost equal the normal force of the tripod has an interesting structure (see Fig. 3). The tripod can also rotate and slide with stability until a time near the end of its motion, at which point the motion becomes unstable and the tripod tips.

We compare the tripod trajectories to trajectories of rotating, sliding cylinders that have continuous contact rings. We find that these trajectories can be almost the same for the extremes of "slow" rotation and "rapid" rotation, which supports results reported in previous works. Moreover, when the translational speed and rotational speed are almost the same, we find that the trajectories of the tripod and a cylinder having a continuous contact ring are, in general, almost the same.

We also discuss significant implications of our results, including: normal forces and motions of cylinders with more than three contact points; comparison of the exact normal force for the tripod with the normal force around a continuous contact ring; the motion of a flat, smooth sheet of material sliding over a number of identical spheres.

We find no material in the literature about the motion of a rotating, sliding tripod. There are, however, a number of papers that study the motion of sliding, rotating cylinders and disks that have smooth contact patterns [4–16].

2. Equations of motion

We study the motion of a tripod with total mass M uniformly distributed in a circular cylinder of height H and radius R. The tripod rotates and slides on a smooth surface, and has three legs that make contact with the surface. For convenience, we take the contact points to be 120° apart and located on a circle of radius r whose center is directly beneath the CM. The cylindrical symmetry simplifies the calculations while retaining important physical features. The CM is at a height h above the surface and located on the axis of symmetry of the circular cylinder, which also passes through the center of the circle of radius r. We take the coefficient of friction to have a constant value μ.

The force exerted on each leg is the sum of the normal force $\boldsymbol{N}_i$ and the force of friction $\boldsymbol{F}_i$, where $i = 1, 2, 3$ for the three legs. The *only* assumptions we make are that the magnitude F_i of $\boldsymbol{F}_i$ is μN_i and that the direction of $\boldsymbol{F}_i$ is opposite to the instantaneous direction of motion $\boldsymbol{u}_i$ of the contact point of leg i relative to the surface.

Fig. 1. Overhead view of the initial configuration of the tripod. The y-axis is in the direction of the initial velocity $\boldsymbol{v}_0$ of the CM of the tripod and the tripod is set spinning counter-clockwise with initial angular velocity $\boldsymbol{\omega}_0$. The initial angle between the positive x-axis and the first leg of the tripod is θ_0. The tripod has a total mass M uniformly distributed in a circular cylinder of height H and radius R. The contact points are 120° apart and located on a circle of radius r whose center is located directly beneath the CM of the tripod.

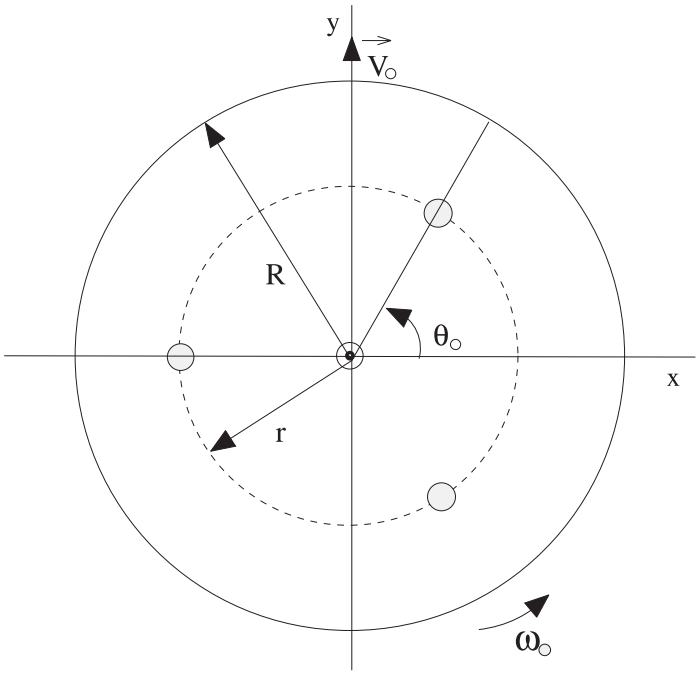

We define an inertial frame as follows: the y-axis is in the direction of the initial velocity $\boldsymbol{v}_0$ of the CM of the tripod, the x-axis is perpendicular to the y-axis, and the z-axis is normal to and away from the surface. We also define a sequence of instantaneous inertial frames with unit vectors $\hat{e}_v$ and $\hat{e}_\mathrm{T}$ such that $\hat{e}_v$ is in the direction of the instantaneous velocity $\boldsymbol{v}(t)$ of the CM, $\hat{e}_\mathrm{T}$ is transverse to $\hat{e}_v$, with $\hat{e}_\mathrm{T} \times \hat{e}_v = \hat{e}_z$, where $\hat{e}_z$ is a unit vector in the positive z direction. Note that the origins of the instantaneous inertial frames are located on the surface and directly beneath the instantaneous positions of the CM.

The initial angle between the positive x-axis and the first leg of the tripod, θ_0, specifies the initial locations of the tripod's legs, and is in the range $0 \leq \theta_0 < 2\pi/3$. At later times, the angle θ_1 of the first leg is measured from the positive $\hat{e}_\mathrm{T}$ axis to the first leg of the tripod in the instantaneous inertial frame. The tripod is given an initial velocity $\boldsymbol{v}_0$ and set spinning counter-clockwise with initial angular speed ω_0. The magnitudes of the instantaneous velocity and angular velocity are given by v and ω, respectively. An overhead view of the initial configuration of the tripod is given in Fig. 1 and an overhead view of the tripod in the instantaneous inertial frame including the forces and torques on one of the tripod legs is given in Fig. 2.

For smooth motion, we require that the tripod legs always remain in full contact with the surface. Any net force in the vertical direction would cause the tripod to accelerate away from the surface and any net torque in the plane would cause the tripod to tip. This implies that the forces on the legs of the tripod are such that the net force in the z direction is zero and that the net torques in the $\hat{e}_\mathrm{T}$ and $\hat{e}_v$

Fig. 2. Forces and torques in the instantaneous inertial frame acting on one of the contact points of the tripod. The physical quantities are as follows: $\boldsymbol{v}$ is the velocity of the CM of the tripod; $\boldsymbol{v}_{\rm rot}$ is the rotational velocity of the contact point; $\boldsymbol{u} = \boldsymbol{v} + \boldsymbol{v}_{\rm rot}$ is the instantaneous velocity of the contact point relative to the underlying smooth surface. The friction $\boldsymbol{F}_f$ is in the direction opposite to $\boldsymbol{u}$ and has magnitude μN where μ is the coefficient due to friction and $\boldsymbol{N}$ is the normal force acting on the contact point. The friction gives rise to a torque that has a component $\boldsymbol{\tau}_f$ in the $\hat{e}_v - \hat{e}_{\rm T}$ plane, as shown; $\boldsymbol{\tau}_N$ denotes the torque due to the normal force. The tail of the vector $\boldsymbol{r}$ is at the center of the circle on which the contact points lie. The contact point is located at the tip of the vector $\boldsymbol{r}$. The angles θ and η are used in the calculations as described in the text.

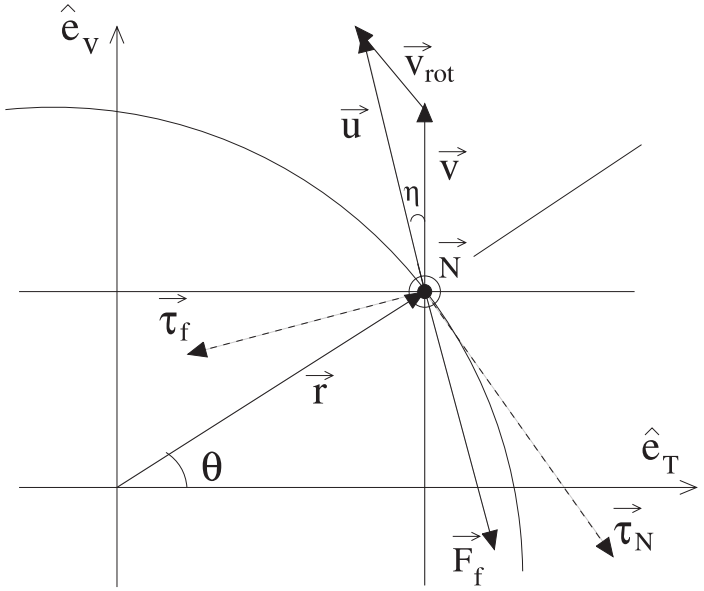

directions are zero. The stability equations for smooth motion are therefore

$$F_z = 0, \qquad \tau_{\rm T} = 0, \qquad \tau_v = 0 \tag{1}$$

Stable motion will allow net forces in the plane of the surface and a net torque in the vertical direction. The equations of motion for the tripod are therefore

$$F_T = Ma_{\rm T}, \qquad F_v = Ma_v, \qquad \tau_z = I\alpha_z \tag{2}$$

where $F_{\rm T}$ is the force in the direction transverse to the direction of motion, F_v is the force in the direction of motion, and τ_z is the torque in the z direction. The variables $a_{\rm T}$ and a_v are the accelerations in the $\hat{e}_{\rm T}$ and $\hat{e}_v$ directions, respectively, and α_z is the angular acceleration in the z direction. Since the mass is uniformly distributed throughout the cylinder, the moment of inertia I is given by $I = \frac{1}{2}MR^2$.

The three stability equations allow us to completely solve for the motion of the tripod. By requiring that the contributions to F_z from the three legs add to Mg, and that the contributions to $\tau_{\rm T}$ and τ_v from the three legs add to zero, we can solve for the normal forces on the three legs (three equations in three unknowns). This is why the tripod is a unique case — if we had four legs we would have the same three stability equations but *four* unknowns. We will discuss this further later in the paper. Once the normal forces are known, we can calculate the forces $F_{\rm T}$ and F_v and the torque τ_z. Then, using the equations of motion (2), one can completely describe the motion of the tripod. To illustrate how one finds the normal forces N_1, N_2, and N_3 on legs one, two, and three of the tripod, respectively, we consider the

case where $v > r\omega$ and the tripod legs are located in quadrants I, II, and III. Referring to Fig. 2, we find the following forces and torques on the tripod leg in quadrant I:

$$\tau_{\mathrm{T}}^{(1)} = +rN_1 \sin\theta_1 - \mu h N_1 \cos\left[\eta_+(\theta_1)\right] \tag{3}$$

$$\tau_{v}^{(1)} = -rN_1 \cos\theta_1 - \mu h N_1 \sin\left[\eta_+(\theta_1)\right] \tag{4}$$

$$\tau_{z}^{(1)} = -r\mu N_1 \cos\left[\theta_1 - \eta_+(\theta_1)\right] \tag{5}$$

$$F_{\mathrm{T}}^{(1)} = +\mu N_1 \sin\left[\eta_+(\theta_1)\right] \tag{6}$$

$$F_{v}^{(1)} = -\mu N_1 \cos\left[\eta_+(\theta_1)\right] \tag{7}$$

$$F_{z}^{(1)} = N_1 \tag{8}$$

where

$$\eta_{\pm}(\theta) = \tan^{-1}\left(\frac{r\omega\sin\theta}{v \pm r\omega\cos\theta}\right) \tag{9}$$

and $0 \leq \theta_1 < \pi/3$ to guarantee that quadrant IV has no contact point. In a similar fashion we find the forces and torques on the tripod leg in quadrant II:

$$\tau_{\mathrm{T}}^{(2)} = +rN_2 \sin\theta_2 - \mu h N_2 \cos\left[\eta_-(\theta_2)\right] \tag{10}$$

$$\tau_{v}^{(2)} = +rN_2 \cos\theta_2 - \mu h N_2 \sin\left[\eta_-(\theta_2)\right] \tag{11}$$

$$\tau_{z}^{(2)} = +r\mu N_2 \cos\left[\theta_2 + \eta_-(\theta_2)\right] \tag{12}$$

$$F_{\mathrm{T}}^{(2)} = +\mu N_2 \sin\left[\eta_-(\theta_2)\right] \tag{13}$$

$$F_{v}^{(2)} = -\mu N_2 \cos\left[\eta_-(\theta_2)\right] \tag{14}$$

$$F_{z}^{(2)} = N_2 \tag{15}$$

where θ_2 is the angle measured from the negative $\hat{e}_{\mathrm{T}}$ axis to the second tripod leg. We require $\pi/6 < \theta_2 \leq \pi/3$ to ensure that quadrant IV has no contact point. The forces and torques on the tripod leg in quadrant III are given by

$$\tau_{\mathrm{T}}^{(3)} = -rN_3 \sin\theta_3 - \mu h N_3 \cos\left[\eta_-(\theta_3)\right] \tag{16}$$

$$\tau_{v}^{(3)} = +rN_3 \cos\theta_3 + \mu h N_3 \sin\left[\eta_-(\theta_3)\right] \tag{17}$$

$$\tau_{z}^{(3)} = +r\mu N_3 \cos\left[\theta_3 + \eta_-(\theta_3)\right] \tag{18}$$

$$F_{\mathrm{T}}^{(3)} = -\mu N_3 \sin\left[\eta_-(\theta_3)\right] \tag{19}$$

$$F_{v}^{(3)} = -\mu N_3 \cos\left[\eta_-(\theta_3)\right] \tag{20}$$

$$F_{z}^{(3)} = N_3 \tag{21}$$

where θ_3 is the angle measured from the negative $\hat{e}_{\mathrm{T}}$ axis to the third tripod leg. We require $\pi/3 \leq \theta_3 < \pi/2$ to ensure that quadrant IV has no contact point. We note that the equations above can all be written in terms of a single angle because the tripod legs are evenly spaced. For example, to write the equations in terms of θ_1 only, we use the relations $\theta_2 = \pi/3 - \theta_1$ and $\theta_3 = \pi/3 + \theta_1$, which can be found readily

from the definitions of θ_2 and θ_3. The stability equations (1) can be applied to the case described above to yield

$$N_1 + N_2 + N_3 - Mg = 0 \tag{22}$$

$$a_1 N_1 + a_2 N_2 + a_3 N_3 = 0 \tag{23}$$

$$b_1 N_1 + b_2 N_2 + b_3 N_3 = 0 \tag{24}$$

where $g = 9.81$ m/s^2 is the acceleration due to gravity and

$$a_1 = +r\sin(\theta_1) - \mu h\cos\left[\eta_+(\theta_1)\right] \tag{25}$$

$$a_2 = +r\sin(\theta_2) - \mu h\cos\left[\eta_-(\theta_2)\right] \tag{26}$$

$$a_3 = -r\sin(\theta_3) - \mu h\cos\left[\eta_-(\theta_3)\right] \tag{27}$$

$$b_1 = -r\cos(\theta_1) - \mu h\sin\left[\eta_+(\theta_1)\right] \tag{28}$$

$$b_2 = +r\cos(\theta_2) - \mu h\sin\left[\eta_-(\theta_2)\right] \tag{29}$$

$$b_3 = +r\cos(\theta_3) + \mu h\sin\left[\eta_-(\theta_3)\right] \tag{30}$$

where $\theta_2 = \pi/3 - \theta_1$ and $\theta_3 = \pi/3 + \theta_1$ in (25)–(30). Solving for the normal forces is straightforward. We find that

$$N_1 = \frac{a_3 b_2 - a_2 b_3}{(a_2 - a_3)b_1 + (a_3 - a_1)b_2 + (a_1 - a_2)b_3} Mg \tag{31}$$

$$N_2 = \frac{a_1 b_3 - a_3 b_1}{(a_2 - a_3)b_1 + (a_3 - a_1)b_2 + (a_1 - a_2)b_3} Mg \tag{32}$$

$$N_3 = \frac{a_2 b_1 - a_1 b_2}{(a_2 - a_3)b_1 + (a_3 - a_1)b_2 + (a_1 - a_2)b_3} Mg \tag{33}$$

Note that these expressions for the normal forces on the three legs are valid when quadrant IV has no contact point. To completely describe the normal forces for all values of θ, we need to also look at the cases where quadrants III, II, and I have no contact points. These correspond to regions of θ_1 given by $\pi/6 \leq \theta_1 < \pi/3$ (quadrant III has no contact point), $\pi/3 \leq \theta_1 < \pi/2$ (quadrant II has no contact point), and $\pi/2 \leq \theta_1 < 2\pi/3$ (quadrant I has no contact point). A similar calculation to that presented above is done in each case and the normal forces are found on each of the three legs. Piecing together the normal force on the first leg in the range $0 \leq \theta_1 < 2\pi/3$ and the normal force on the second leg in the range $2\pi/3 \leq \theta_2 < 4\pi/3$ and the normal force on the third leg in the range $4\pi/3 \leq \theta_3 < 2\pi$, we obtain the normal force for all θ from 0 to 2π.

However, some simplification is possible. We find that taking the normal force found for the first region ($0 \leq \theta_1 < \pi/6$) over all angles from 0 to 2π reproduces the piecewise normal force described above. This result was expected because the forces and torques calculated in quadrant I of Fig. 2 should change sign accordingly when extended into the other quadrants. This confirms our calculations to this stage. We next write the following expressions for the normal forces that are valid for any tripod leg in the range from $0 \leq \theta_1 < 2\pi$ where θ_1 is measured counter-clockwise from the positive $\hat{e}_\mathrm{T}$ axis:

$$N_{v>r\omega} = \frac{a_3 b_2 - a_2 b_3}{(a_2 - a_3)b_1 + (a_3 - a_1)b_2 + (a_1 - a_2)b_3} Mg \tag{34}$$

and

$$N_{v<r\omega} = \frac{c_3 d_2 - c_2 d_3}{(c_2 - c_3)d_1 + (c_3 - c_1)d_2 + (c_1 - c_2)d_3} Mg \tag{35}$$

Fig. 3. For $r\omega$ close to v, the normal force exhibits an interesting structure. The continuous curve is for $s \equiv r\omega/v = 1.01$; the broken curve is for $s = 0.99$. The parameter $\alpha \equiv \mu h/r = 0.1$ in both curves. Note that the normal force at the front of the tripod ($0 \leq \theta \leq \pi$) is greater than that at the back of the tripod ($\pi \leq \theta \leq 2\pi$). The structure near $\theta = \pi/3$, $\theta = \pi$, and $\theta = 5\pi/3$ is discussed in the text.

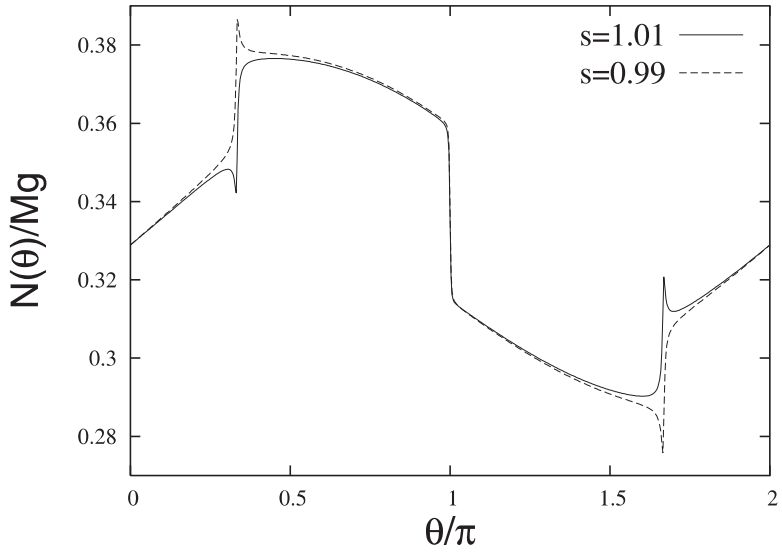

where

$$c_1 = +r\sin(\theta_1) - \mu h\cos\left[\theta_1 - \nu_+(\theta_1)\right] \tag{36}$$

$$c_2 = +r\sin(\theta_2) + \mu h\cos\left[\theta_2 + \nu_-(\theta_2)\right] \tag{37}$$

$$c_3 = -r\sin(\theta_3) + \mu h\cos\left[\theta_3 + \nu_-(\theta_3)\right] \tag{38}$$

$$d_1 = -r\cos(\theta_1) - \mu h\sin\left[\theta_1 - \nu_+(\theta_1)\right] \tag{39}$$

$$d_2 = +r\cos(\theta_2) - \mu h\sin\left[\theta_2 + \nu_-(\theta_2)\right] \tag{40}$$

$$d_3 = +r\cos(\theta_3) + \mu h\sin\left[\theta_3 + \nu_-(\theta_3)\right] \tag{41}$$

and

$$\nu_\pm(\theta) = \tan^{-1}\left(\frac{v\sin\theta}{r\omega \pm v\cos\theta}\right) \tag{42}$$

where, for convenience, θ_1 designates the location of any leg (in the range $0 \leq \theta_1 < 2\pi$), $\theta_2 = \pi/3 - \theta_1$ and $\theta_3 = \pi/3 + \theta_1$.

Plots of the normal force versus θ show that, as expected, the normal force is greater at the "front" of the tripod than it is at the "back". The normal force $N(\theta)$ has interesting structure when $r\omega/v$ is close to one as shown in Fig. 3.

The structure of the normal force near $\theta = \pi/3, \pi, 5\pi/3$ when $r\omega \approx v$ can be understood by examining the force of friction $\boldsymbol{F}_f^{(2)}$ on leg 2 near $\theta = \pi$ and the torque $\boldsymbol{\tau}_f^{(2)}$ due to $\boldsymbol{F}_f^{(2)}$. Consider first the case where the angle θ_2 for leg 2 is slightly less than π, as measured from the positive $\hat{e}_\mathrm{T}$ axis. The direction of motion of the contact point relative to the surface is given by $\boldsymbol{u}^{(2)} = \boldsymbol{v} + \boldsymbol{v}_\mathrm{rot}^{(2)}$ with $|\boldsymbol{v}_\mathrm{rot}^{(2)}| = r\omega$. For θ_2 slightly smaller than π, the direction of $\boldsymbol{u}^{(2)}$ will be very close to the negative $\hat{e}_\mathrm{T}$

direction, giving a torque in the $\hat{e}_v - \hat{e}_T$ plane of magnitude $r\mu N_2$ in the *negative* $\hat{e}_v$ direction. For θ_2 slightly greater than π, $\boldsymbol{u}^{(2)}$ is close to being in the positive $\hat{e}_T$ direction, and the torque of magnitude $r\mu N_2$ is in the *positive* $\hat{e}_v$ direction. Thus, the torque goes from $-r\mu N_2\hat{e}_v$ to $+r\mu N_2\hat{e}_v$ when θ_2 goes from just slightly less than π to slightly more than π. This large change through a small angle of rotation is the reason for the structure in Fig. 3.

A straightforward calculation gives the following expressions for the normal forces in the special case $v = r\omega$ when the second tripod leg is at an angle $\pi^{\pm}$:

$$N\left(\frac{\pi^{\pm}}{3}\right) = \frac{1 + \alpha \pm \alpha \pm \alpha^2}{3 \pm 2\alpha + \alpha^2} Mg \tag{43}$$

$$N\left(\pi^{\pm}\right) = \frac{1 + \alpha^2}{3 \pm 2\alpha + \alpha^2} Mg \tag{44}$$

$$N\left(\frac{5\pi^{\pm}}{3}\right) = \frac{1 - \alpha \pm \alpha \mp \alpha^2}{3 \pm 2\alpha + \alpha^2} Mg \tag{45}$$

where the symbol $^{\pm}$ refers to the limits from the right and the left, respectively. In Fig. 3, $\alpha = \mu h/r = 0.1$, giving the following values for $N(\theta)/Mg$:

θ	$\pi/3^-$	$\pi/3^+$	π^-	π^+	$5\pi/3^-$	$5\pi/3^+$
N/Mg	0.352	0.377	0.359	0.315	0.288	0.308

We also find that the normal force on the legs of the tripod has simple asymptotic forms when the rotation is very rapid and also when the rotation is very slow:

$$N(\theta) \to \frac{1}{3}\left(1 + a\sin\theta + b\cos\theta\right) Mg, \qquad v \ll r\omega \tag{46}$$

$$N(\theta) \to \frac{1}{3}\left(1 + \frac{2\mu h}{r}\sin\theta\right) Mg, \qquad v \gg r\omega \tag{47}$$

where

$$a = \frac{\left(\frac{\mu h}{r}\right)\left(\frac{v}{r\omega}\right)}{1 + \left(\frac{\mu h}{r}\right)^2} \qquad b = -\frac{\left(\frac{\mu h}{r}\right)^2\left(\frac{v}{r\omega}\right)}{1 + \left(\frac{\mu h}{r}\right)^2} \tag{48}$$

We can write the equations for the net force on the tripod in the instantaneous inertial frame. We recall that the force in the direction of the instantaneous velocity is F_v, the force transverse to the instantaneous velocity is F_T, and the torque in the z direction is τ_z. There are again eight cases that depend on which quadrant has no contact point and if $r\omega < v$ or $r\omega > v$. We do not list all of these cases explicitly but note that in each case we find F_T, F_v, and τ_z and each of these depends on three quantities that arise from the contribution of each leg of the tripod. For the case of $v > r\omega$ and quadrant IV having no contact point, we find

$$F_T = +\mu N(\theta_a)\sin\left[\eta_+(\theta_1)\right] + \mu N(\theta_b)\sin\left[\eta_-(\theta_2)\right] - \mu N(\theta_c)\sin\left[\eta_-(\theta_3)\right] \tag{49}$$

$$F_v = -\mu N(\theta_a)\cos\left[\eta_+(\theta_1)\right] - \mu N(\theta_b)\cos\left[\eta_-(\theta_2)\right] - \mu N(\theta_c)\cos\left[\eta_-(\theta_3)\right] \tag{50}$$

$$\tau_z = -r\mu N(\theta_a)\cos\left[\theta_1 - \eta_+(\theta_1)\right] + r\mu N(\theta_b)\cos\left[\theta_2 + \eta_-(\theta_2)\right] + r\mu N(\theta_c)\cos\left[\theta_3 + \eta_-(\theta_3)\right] \tag{51}$$

where θ_a, θ_b, and θ_c are the angles to the first, second, and third legs of the tripod, respectively, measured counter-clockwise from the positive $\hat{e}_{\mathrm{T}}$ axis and $\theta_1 = \theta_a$, $\theta_2 = \pi/3 - \theta_1$, and $\theta_3 = \pi/3 + \theta_1$.

Now that the *exact* expressions for the normal forces, net force, and torque are known, we can derive the equations of motion of the tripod. To proceed, we choose a sequence of inertial frames such that, at any time t, $\hat{e}_v$ is in the instantaneous direction of motion, $\hat{e}_{\mathrm{T}}$ is transverse to $\hat{e}_v$, and $\psi(t)$ is the angle between the initial direction of motion and the instantaneous velocity. The angle $\psi(t)$ can be written explicitly as

$$\psi(t) = \tan^{-1}\left[\frac{v_x(t)}{v_y(t)}\right] \tag{52}$$

To translate from the instantaneous inertial frame back to the fixed inertial frame we use

$$F_x(t) = +F_{\mathrm{T}}\cos[\psi(t)] + F_v \sin[\psi(t)] \tag{53}$$

$$F_y(t) = -F_{\mathrm{T}}\sin[\psi(t)] + F_v \cos[\psi(t)] \tag{54}$$

These equations are easily derived [4]. Using the equations of motion (2), we can integrate to find the velocity and angular velocity as a function of time:

$$v_x(t) = \frac{1}{M}\int_0^t F_x(t')\,\mathrm{d}t' \tag{55}$$

$$v_y(t) = v_0 + \frac{1}{M}\int_0^t F_y(t')\,\mathrm{d}t' \tag{56}$$

$$w(t) = w_0 + \frac{1}{I}\int_0^t \tau_z(t')\,\mathrm{d}t' \tag{57}$$

Integrating again we obtain the position of the tripod as a function of time:

$$x(t) = \int_0^t v_x(t')\,\mathrm{d}t' \tag{58}$$

$$y(t) = \int_0^t v_y(t')\,\mathrm{d}t' \tag{59}$$

We have succeeded in obtaining the exact formulae that describe the motion of a rotating tripod sliding over a smooth surface with no approximations.

3. Results

To proceed with a tripod run, we fix the parameters r, R, h, and μ. We set the initial values of x_0, y_0, v_0, ω_0, and $\theta_0 = \theta_1$ at $t = t_0$ and then use a numerical program that uses (55)–(59) to calculate the following quantities: $x(t)$, $y(t)$, $\omega(t)$, $F_v(t)$, $F_{\mathrm{T}}(t)$, $\tau_z(t)$, $N_1(t)$, $N_2(t)$, $N_3(t)$, $T_{\mathrm{trans}}(t)$, and $T_{\mathrm{rot}}(t)$, where $T_{\mathrm{trans}}(t)$ and $T_{\mathrm{rot}}(t)$ are the kinetic energies of translation and rotation, respectively.

We consider first the case of rapid rotation and slow sliding, i.e., $r\omega \gg v$. The tripod's CM follows "looping" trajectories as shown in Fig. 4. In the limit of extremely rapid rotation and a somewhat large value of $\mu h/r$, we obtain nearly circular trajectories for the tripod. We compare the rapidly rotating tripod results to the results reported previously [4] for a rapidly rotating circular cylinder having a continuous circular contact ring. We will refer to a circular cylinder having a continuous circular contact ring as a CCR hereafter. We look specifically at a special case described in ref. 4 that produces a purely analytical result for the trajectory of a rapidly rotating CCR. Comparisons of the trajectories for a rapidly rotating tripod and a CCR are shown in Fig. 4 for increasing values of $s = r\omega_0/v_0$. The first set of plots is for

Fig. 4. Comparison of the trajectories of a rapidly rotating tripod (broken curve) and a rapidly rotating cylinder with a circular contact ring (continuous curve). The trajectories are for $s = r\omega_0/v_0 = 5$, 10, 15, 20 with $v_0 = 2.5$ m/s, $\theta_0 = 0$, $r = 0.0625$ m, $h = 0.625$ m, and $\mu = 0.5$. The values of R change slightly with the value of s. See text for details.

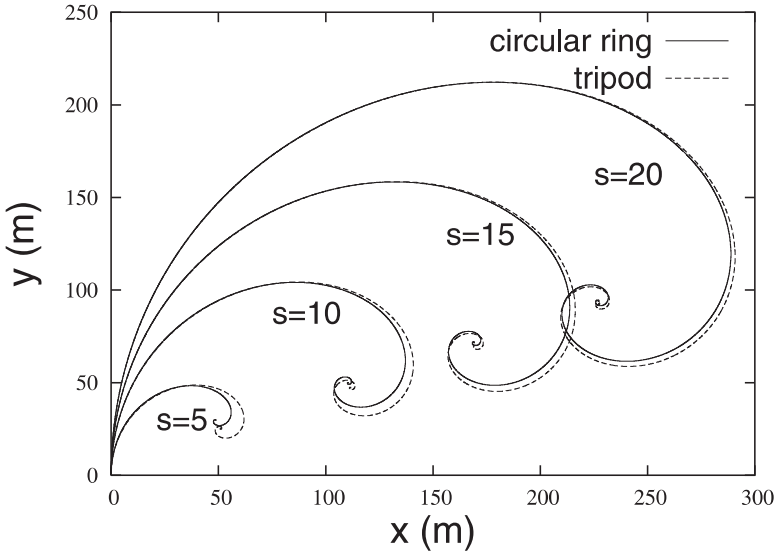

$s = 5$ and we require the ratio $R/r = 8.32$ to use the analytical result for the CCR from ref. 4. The second plot is for $s = 10$ and we require the ratio $R/r = 9.6$. Similarly the plots for $s = 15$ and $s = 20$ require the ratios $R/r = 9.92$ and $R/r = 10.08$, respectively.

We expect a rapidly rotating tripod to give results similar to a rapidly rotating CCR because the rapidly rotating tripod samples all the angles in a circle of radius r during a very small time, thus simulating a rapidly rotating CCR. The trajectories are in very good agreement. We note that the deviation between the trajectories occurs near the end of the motion. A possible explanation for this is that, near the end of the run, the tripod has slowed down considerably due to friction and will no longer sample all angles over a short time and thus will no longer exhibit the behaviour of the sliding, rotating CCR.

The agreement in Fig. 4 for the trajectories of a tripod as compared to a CCR indicates that the normal force for the latter can be taken to be the same, or almost the same, as the normal force for the tripod. It is important to recognize that the normal force $N_{\mathrm{CCR}}(\theta)$ for such a cylinder cannot be calculated for a continuum of contact points at all points θ in the range 0 to 2π. Instead, one *assumes* that $N_{\mathrm{CCR}}(\theta) = N_{\mathrm{tripod}}(\theta)$. Such an assumption seems reasonable.[2] Further discussion is given in the next section of this paper.

We next look at the behaviour of the tripod in the slowly rotating regime ($r\omega \ll v$). We again compare the tripod and CCR trajectories. Here, we do not necessarily expect the trajectories to match because the tripod does not sample all angles in a short time and might not exhibit the behaviour of a CCR. Comparison of the trajectories in the slowly rotating regime are given in Fig. 5; the trajectory for the CCR is given by analytical expressions derived in ref. 5.

That the two trajectories in Fig. 5 are so close is significant. Given that the rotation is slow, and, therefore, that the tripod does not sample all angles, it is not unquestionably expected that the trajectories

[2]For $N_{\mathrm{CCR}}(\theta) = N_{\mathrm{tripod}}(\theta)$, given that $\tau_v = 0$ and $\tau_{\mathrm{T}} = 0$ for the tripod, it automatically follows that $\tau_v = 0$ and $\tau_{\mathrm{T}} = 0$ for the CCR.

Fig. 5. Comparison of the trajectories of a tripod (broken curve) and of a cylinder (continuous curve) with $s = r\omega_0/v_0 = 0.1$, $v_0 = 5.0$ m/s, $\theta_0 = 0$, $r = 0.0625$ m, $R = 0.14$ m, $h = 0.0625$ m, and $\mu = 0.25$. Note that the two trajectories are very close. The values of x_{final} and y_{final} are almost the same for the two trajectories. See text for full discussion.

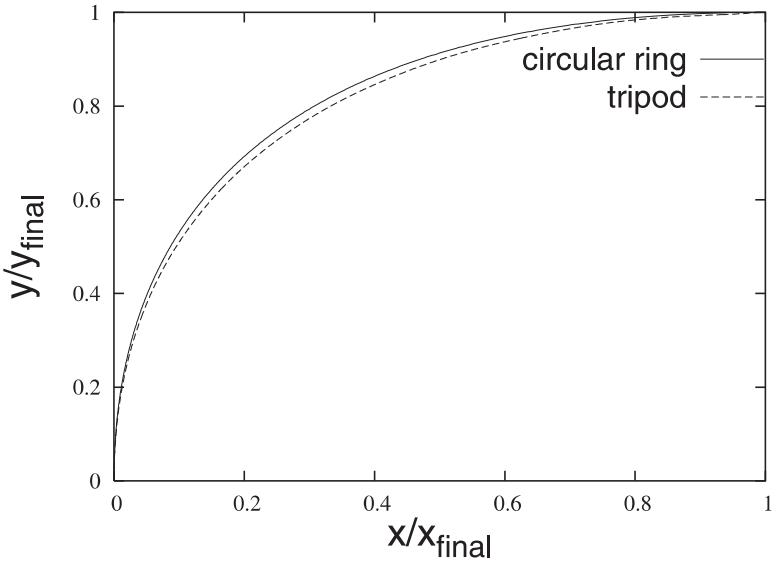

agree. That they do agree supports the use of the normal force $N_{\text{tripod}}(\theta)$ for the CCR. Moreover, the trajectories of the tripod and the CCR are in good agreement even when $r\omega$ and v are almost equal. The implications of this agreement go beyond this, and we will discuss this more fully in the next two sections of this paper.

We also point out that a cylinder with a flat, circular contact area, with radius r and area πr^2, will not follow the same trajectory as the tripod with radius r or the CCR with radius r, given the same initial conditions.

We find additional novel physical features. The first example is serpentine paths for the CM of the tripod. A serpentine trajectory is shown in Fig. 6.

In this plot, we see that the motion of the tripod has oscillations in the lateral direction of motion. Even more peculiar is the complete reversal in the lateral direction toward the end of the run. Trajectories of a similar serpentine form are seen for a number of tripod runs where the ratio h/r is small. In Fig. 6 this ratio is 0.07.

The serpentine trajectory can be understood using the following picture. Consider having two of the contact points in the back (quadrants III and IV) and the other contact point in the front (quadrant I or II). For a counter-clockwise, rotating, sliding tripod the force of friction on the front contact point has its $\hat{e}_{\text{T}}$ component in the *positive* $\hat{e}_{\text{T}}$ direction whereas the forces of friction on the back contact points have their $\hat{e}_{\text{T}}$ components in the *negative* $\hat{e}_{\text{T}}$ direction. The component of the net force of friction in the $\hat{e}_{\text{T}}$ direction is *negative*, causing the tripod to curve to the left. Indeed for both swings to the left in Fig. 6 there are two contact points in the back and one contact point in the front. During both swings the contact point in quadrant III goes from slightly more than 180° to approximately 240° and the point in quadrant IV goes from about −60° to 0°. Also, the contact point in the front goes from about 60° to 120°.

For the initial conditions of Fig. 6, the trajectory of a CCR was found to be a smooth curve, as expected. This shows that the serpentine nature of the trajectory of a tripod is directly due to the tripod having only three contact points.

Fig. 6. Serpentine trajectory of a tripod. The parameters are $s = r\omega_0/v_0 = 0.45$, $v_0 = 1.0$ m/s, $\theta_0 = 0$, $r = 0.0625$ m, $R = 0.069$ m, $h = 0.0044$ m, and $\mu = 0.1$. The explanation is given in the text.

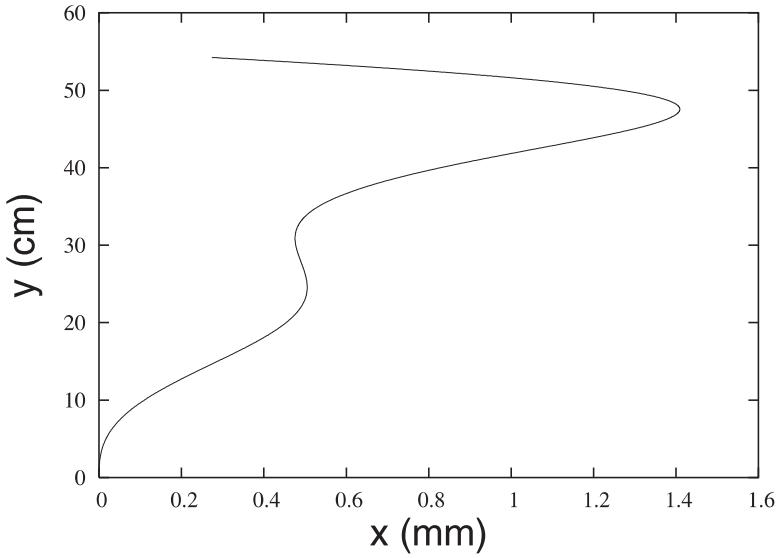

For a suitable choice of parameters we find that the translational kinetic energy of the tripod oscillates. Plots of the translational, rotational, and total kinetic energies versus time are shown in Fig. 7.

Oscillations in the translational kinetic energy are found in tripod runs where the ratio $\mu h/r$ is large and the kinetic energy is low. In Fig. 7, the ratio $\mu h/r$ is 5.0.

This effect can be understood with the following picture. Consider having two of the contact points on the "left" (quadrants II and III) and the other contact point on the "right" (quadrant I or IV). Note from Fig. 7 that $r\omega_0 = 3v_0$, i.e., the rotational speed is significantly larger than the sliding speed. For a counter-clockwise rotating, sliding tripod the force of friction on the right contact point has its $\hat{e}_v$ component in the *negative* $\hat{e}_v$ direction whereas the forces of friction on the left contact points have their $\hat{e}_v$ components in the *positive* $\hat{e}_v$ direction. The component of the net force of friction in the $\hat{e}_v$ direction is *positive*, giving the tripod a "push", increasing its translational kinetic energy. However, over any full cycle of rotation the translational kinetic energy decreases as shown in Fig. 7*a*. Note that this requires $r\omega$ to be significantly larger than v, as a simple sketch will illustrate.

We emphasize that the oscillations in Fig. 7*a* are *not* due to numerical round-off errors. Indeed, $T_{\rm rot}(t)$ is monotonic nonincreasing in time in all cases studied, and $T_{\rm total}(t) \equiv T_{\rm trans}(t) + T_{\rm rot}(t)$ is monotonic decreasing in time even through a single full rotation and even on a time scale smaller than that of Fig. 7.

We see that the *translational* kinetic energy, $T_{\rm trans}(t)$, can oscillate in time, which would seem to imply that the *rotational* kinetic energy, $T_{\rm rot}(t)$, must also oscillate in time. Consider the magnitudes of the translational and rotational kinetic energies shown in Fig. 7: as t increases from 0.4 s to 0.5 s, the oscillations in $T_{\rm trans}(t)$ are of order 0.01 J, whereas the drop in $T_{\rm rot}(t)$ during this time is slightly more than 6 J. The drop in $T_{\rm rot}(t)$ is so rapid that, despite the small oscillations in $T_{\rm trans}(t)$, the total kinetic energy is monotonically decreasing in time, even though $T_{\rm rot}(t)$ itself does not have oscillations. This is readily understood by considering the following function $y(x)$: $y(x) = -x + \epsilon \sin(x)$ with $0 < \epsilon \ll 1$; we have that the slope is $dy/dx = -1 + \epsilon \cos(x)$, which is always negative provided $0 < \epsilon < 1$. Thus, $T_{\rm total}(t)$ and $T_{\rm rot}(t)$ can both be monotonically decreasing in time while $T_{\rm trans}(t)$ exhibits small oscillations, all of which are manifest in Fig. 7.

The tripod can be found to tip at a very late stage of its motion. For several runs, we found that

Fig. 7. The kinetic energies of the tripod as a function of time. The parameters are $s = r\omega_0/v_0 = 3.0$, $v_0 = 6.25$ m/s, $\theta_0 = 0$, $r = 0.0625$ m, $R = 0.056$ m, $h = 0.39$ m, and $\mu = 0.8$. Full details are given in the text. (*a*) The translational kinetic energy versus time. (*b*) The rotational kinetic energy versus time. (*c*) The total kinetic energy versus time.

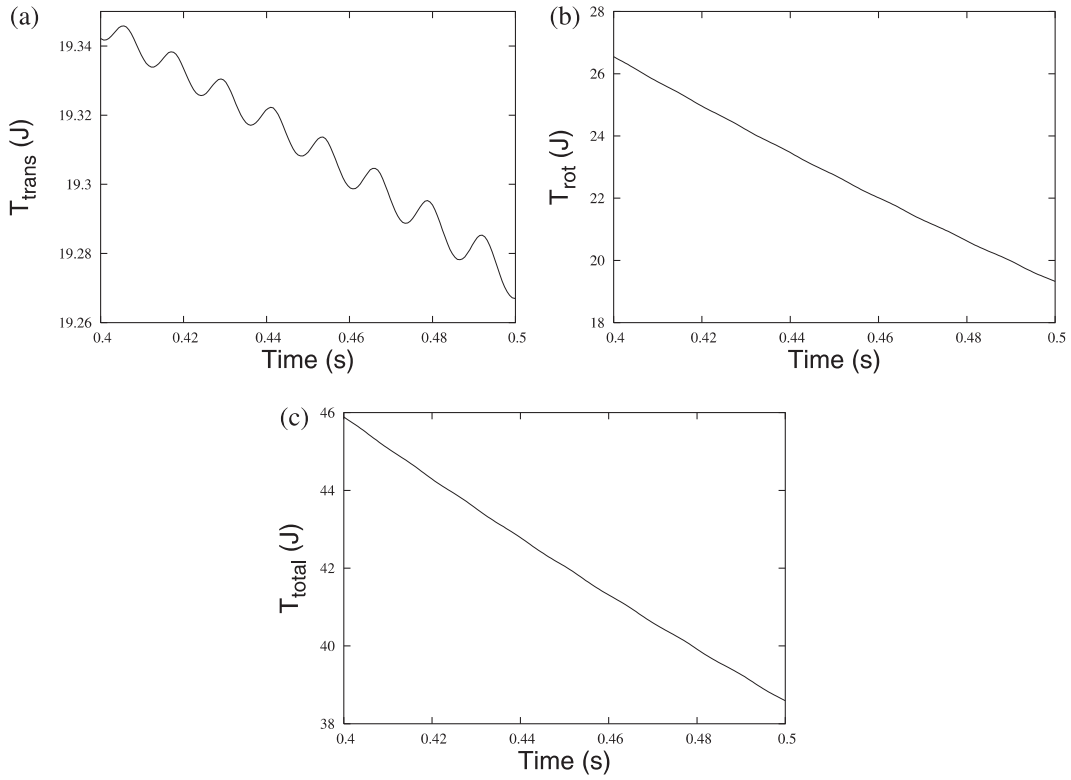

the tripod would exhibit stable motion for a large time and then, near the end of the run, the normal force on one of the three legs would become negative. A negative normal force implies that the surface has to pull on the tripod leg to maintain smooth motion. Since this does not happen, the tripod tips at this point. An example of such a run was found with the following parameters: $s = r\omega_0/v_0 = 30.0$, $v_0 = 6.25$ m/s, $r = 0.0625$ m, $R = 0.19$ m, $h = 0.39$ m, and $\mu = 0.8$. In this particular run, the tripod tips at a time $t \approx 175$ s, at which point the total kinetic energy is only 0.08% of its initial value.

4. Normal force for a circular cylinder with a continuous contact ring

In a previous investigation [4], the motion of an extremely rapidly rotating cylinder sliding slowly (i.e., $r\omega \gg v$) on a smooth surface was studied. The normal force for the continuous contact ring was *assumed* to be the same as the normal force $N_{\text{tripod}}(\theta)$ of the tripod, namely,

$$\mathrm{d}N(\theta) = (1 + a\sin\theta + b\cos\theta)\, Mg\frac{\mathrm{d}\theta}{2\pi} \tag{60}$$

The reasoning behind this assumption was that, in rotating rapidly, the continuous contact ring could be regarded as a huge number of triples of contact points, each triple having contact points 120° apart; thus the normal force on the continuous contact ring could be regarded as being given by the normal force for an extremely rapidly rotating tripod. Similarly, the normal force for a slowly rotating cylinder

($r\omega \ll v$) was taken to have the form of the tripod's normal force, namely: [5]

$$\mathrm{d}N(\theta) = \left(1 + \frac{2\mu h}{r}\sin\theta\right) Mg\frac{\mathrm{d}\theta}{2\pi} \tag{61}$$

The work in this paper supports that assumption.

In light of these extremes, $r\omega \gg v$ and $r\omega \ll v$, consider the normal force shown in Fig. 3, where $r\omega \approx v$. The strange features at $\theta = \pm\pi/3$ and $\theta = \pi$, while readily understood for the tripod, would not seem to be applicable to the case of a CCR. The implicit assumption here is that all of the points in the contact ring play an important role in the motion of the CCR. In the next section, we will consider more carefully this implicit assumption, with the objective of shedding light on the question: what is the normal force $N_{\mathrm{CCR}}(\theta)$ when $r\omega \approx v$?

5. Normal forces and trajectories of N-pods and cylinders with continuous contact rings

One question that emerges from the study of the tripod is: what are the normal forces and trajectories of cylinders having N contact points, where $N \geq 4$? For $N \geq 4$, we have more than three unknowns and only three equations of constraint. Are there additional equations that will hold in general, or is it the case that the N normal forces can vary in an unpredictable manner? Further, how does one calculate the normal force for a cylinder with a continuous contact ring, or other continuous contact patterns? In general, when we are presented with a situation where there are more unknowns than equations dictated by the constraint equations, we have a statically indeterminate system [17]. The purpose of this section is to highlight some implications of such a system by way of two simple experiments.

First, we take the simplest example of a statically indeterminate system: a linear rod supported by three supports. In this case, it is only required that two supports exist for the rod to be held up.

The experiment consists of three precision weigh-scales, a linear rod, three supports and a heavy steel mass to vary the position of the center of mass of the system.

The supports are placed such that two hold the linear rod at the ends and the third support is placed roughly at the center. The heavy mass is placed at a position roughly between two of the three supports. The measurement of the normal force measured by each scale is recorded. The heavy mass is then removed, the scales are zeroed, and the mass is replaced. By taking the sum of the measurements and comparing to the mass itself, the measurements are believed to be highly accurate. The mass is removed and again replaced by hand as accurately as possible to the original position and another measurement of the normal forces is taken. Repeating this procedure 20 times gave measurements for the normal force at each support. The error of the measurements was observed to vary by anywhere from 20 to 80% of the value itself.

Of importance to note here is that the variability is very large. This result suggests that having more supports than necessary to support the rod leads to normal forces that are highly variable and potentially difficult, if not impossible, to predict.

In the second experiment, we examine the next level of complexity from the first experiment. We now consider the case of a plane, held by multiple supports. In this case, if we have a plane that is supported at more than three points, it is a statically indeterminate system. The question we would like to raise at this point is: What is the effect on the normal force distribution under the supports for such a configuration? Are they highly variable for this case, as they are for the linear rod experiment outlined above?

The simple experiment for this case is to take two optically flat pieces of glass (0.635 cm thick, and approximately 15 cm $\times$ 10 cm) and place approximately 15 chrome steel balls between them.[3] The steel balls are used to provide a point contact support.

[3] Precision chrome steel balls were obtained from Kaman Industrial Technologies.

One of the pieces of glass is laid flat on a table, and leveled. The chrome steel balls are dispersed randomly on the glass surface. The second piece of glass is carefully placed on top of the steel balls. Without pushing down on the glass significantly, the top glass plate is pushed in one direction in the plane of the table, and which balls carry the weight of the glass is observed by noting which ones roll with the plate. The result is very counter-intuitive: Only *three* spheres roll with the glass! That is, of the many balls between the plates, only three will be supporting the weight of the plate at any given time.[4] Variation in ball diameter as the cause is discounted by observing that taking the three that roll with the plate at any given time, and moving them to a different location on the plate, it will be a different set of three that roll. Warping of the glass is discounted by flipping the top glass-plate over and repeating. The same was done with the bottom plate. All results indicate that three balls are all that is required, and all that will support the weight of the glass plate, except in situations where sometimes four will support the plate. The fact that four sometimes support the plate is explained by noting that when the center of mass is on, or close to the edge of the triangle formed by the three supports, it is unstable, and may require the fourth for stability over short rolling displacements.

These results are presented to illustrate the complexities in dealing with an N-pod system when $N \geq 4$, and further, for why the tripod is an important structure to investigate.

What are the implications of this experiment? Could it be that the continuous contact ring of a rotating circular cylinder sliding over a smooth surface has only three, or only a small number of points that are actually in contact with the surface at any given time? If so, this would explain why the trajectories of the tripod and the cylinder with a continuous contact ring are almost the same, whether $r\omega \gg v$ or $r\omega \ll v$ or even when the ratio rw/v is of order unity. Moreover, if the motion of the CCR is due to only three or a few contact points when $r\omega \approx v$ then the normal force shown in Fig. 3 *would* be applicable for the motion of the CCR, contrary to what one may well have expected.

We point out that cylinders with CCRs *do* have the same trajectory given the same initial conditions (i.e., the same ω_0 and v_0). If this were not so, the sport of curling [4–9, 13–15], for example, would not be very popular! Again the following question arises: Will an N-pod (e.g., $N = 5$) have, at any given time, only three legs making contact with the surface, or will all N make contact, with variable normal forces? This and related questions can be addressed experimentally.[5]

6. Summary and outlook

In this paper, we investigated the motion of a sliding, rotating tripod, which is unique and important because it is the only sliding, rotating object for which all aspects of the motion can be calculated exactly. We calculated the exact normal forces on the three legs of the tripod and derived the equations of motion for the tripod. The possible trajectories we reported had novel features. For example, a rapidly rotating tripod ($r\omega \gg v$) can execute trajectories with large lateral deflections. We also showed that the tripod can follow serpentine paths; that is, the tripod can start with lateral deflection to the right, for example, and then swing back to the left during its motion. Serpentine paths with even more lateral oscillations are possible. We also found that the *translational* kinetic energy of the tripod can increase during part of the motion while still being monotonically decreasing over full cycles of rotation. When the translational speed and the speed of rotation were almost equal the normal force of the tripod displayed an interesting structure (shown in Fig. 3). For several tripod runs we found that the tripod could exhibit smooth motion for a time until near the end of the motion, at which point the normal force would become negative and the tripod would tip.

We compared the tripod trajectories to trajectories of rotating, sliding cylinders having continuous contact rings. We found that these trajectories can be almost the same for the extremes of slow rotation

[4] In some cases four steel balls move, but only for a very short lateral displacement after which only three steel balls move with the glass plate.

[5] This work is beyond the scope of this paper.

and rapid rotation, which supports results reported in previous works [4–9]. We also found that the trajectories can be quite close when the rotational and translational speeds are comparable. We also discussed significant implications of our results, including normal forces and motions of cylinders with more than three contact points (N-pods). We also compared the exact normal force for the tripod with the normal force for a continuous contact ring. We reported some very interesting observations of the motion of a flat, smooth sheet of material sliding over a number of identical spheres, and raised questions about the motions of N-pods that emerged from these observations.

Acknowledgements

This work was supported by the Natural Sciences and Engineering Research Council of Canada (NSERC). One of us (MRAS) thanks Dr. E.T. Jensen, Dr. Ross Niebergall, and Dr. John S. Hebron for useful discussions. One of us (GLG) acknowledges an NSERC Undergraduate Student Research Award (USRA) and a Postgraduate Scholarship in 2003. Another of us (PB) acknowledges NSERC USRAs in 2003 and 2004. Another of us (RB) acknowledges an NSERC USRA in 2004. We also thank Mr. Mark Lundeberg for examining several hundred numerical runs of tripod motions.

References

1. G.M. Bartenev, V.V. Lavrentjev, and N.A. Konstantinova. Wear, **18**, 439 (1971).
2. X. Shi and A.A. Polycarpou. J. Tribol. Trans. ASME, **125**, 788 (2003).
3. D. Tabor. J. Lub. Tech. **103**, 169 (1981).
4. M.R.A. Shegelski and R. Holenstein. Can. J. Phys. **80**, 141 (2002).
5. M.R.A. Shegelski. Can. J. Phys. **78**, 857 (2000).
6. E.T. Jensen and M.R.A. Shegelski. Can. J. Phys. **82**, 791 (2004).
7. M.R.A. Shegelski and R. Niebergall. Aust. J. Phys. **59**, 1025 (1999).
8. M.R.A. Shegelski and M. Reid. Can. J. Phys. **77**, 903 (1999).
9. M.R.A. Shegelski. Can. J. Phys. **79**, 1117 (2001).
10. K. Voyenli and E. Eriksen. Am. J. Phys. **53**, 1149 (1985).
11. K. Voyenli and E. Eriksen. Am. J. Phys. **54**, 778 (1986).
12. J.M. Daniels. Am. J. Phys. **54**, 777 (1986).
13. G.W. Johnston. Can. Aeronaut. Space J. **27**, 144 (1981).
14. M. Denny. Can. J. Phys. **80**, 1005 (2002).
15. A.R. Penner. Am. J. Phys. **69**, 332 (2001).
16. Z. Farkas, G. Bartels, T. Unger, and D.E. Wolf. Phys. Rev. Lett. **90**, 248302 (2003).
17. I.C. Jong and B.G. Rogers. Engineering Mechanics: Statics and Dynamics. Rinehart and Winston, Inc., Orlando, Fla. Ch. 5. (1991).